REPORT DOCUMENTATION PAGE

Form Approved
OMB No. 0704-0188

1. REPORT DATE *(DD-MM-YYYY)*	**2. REPORT TYPE**	**3. DATES COVERED** *(From - To)*
05/19/2011	Final Report	11/01/2009-01/31/2011

4. TITLE AND SUBTITLE

NUMERICAL STUDY OF 3D FLAPPING WING IN RECTILINEAR AND NON-RECTILINEAR MOTIONS

5a. CONTRACT NUMBER

5b. GRANT NUMBER
FA9550-09-01-0622

5c. PROGRAM ELEMENT NUMBER

6. AUTHOR(S)

Yongsheng Lian

5d. PROJECT NUMBER

5e. TASK NUMBER

5f. WORK UNIT NUMBER

7. PERFORMING ORGANIZATION NAME(S) AND ADDRESS(ES)

University of Louisville
Louisville, KY 40292

8. PERFORMING ORGANIZATION REPORT NUMBER

9. SPONSORING / MONITORING AGENCY NAME(S) AND ADDRESS(ES)

Dr. Douglas R. Smith AFOSR/RSA
Tel: (703) 696-6219 Fax: (703) 696-7320

10. SPONSOR/MONITOR'S ACRONYM(S)

AFOSR

11. SPONSOR/MONITOR'S REPORT NUMBER(S)
AFRL-OSR-VA-TR-2012-0733

12. DISTRIBUTION / AVAILABILITY STATEMENT

Unlimited Distribution

13. SUPPLEMENTARY NOTES

14. ABSTRACT

This report presents the key findings resulting from an AFOSR grant. In this reseasrch we extended our previous results on the linear pitch-ramp-return of a two-dimensional (2D) flat plate to that of a three-dimensional (3D) flat plate of various aspect ratios, in an attempt to quantify 3D effects and the boundary effects on flapping wing aerodynamics. Specifically we compared the leading edge vortex (LEV) between the two-2D and the corresponding 3D cases, and the vortex structure and force histories between a small and a large computational domain. The computational approach solved the incompressible Navier-Stokes equations using a Poisson-like method on overlapping grids. In the computation, the impact of domain size and the presence of walls (as in the experiment) were investigated in particular detail, as earlier work on high-frequency pure-plunge cases has shown remarkable sensitivity of forces to domain size, as well as large differences between wall-bounded and unbounded flows. Comparisons were made with experiments performed at the Air Force Research Laboratory at Wright Patterson. Our study showed that a smaller domain leads to higher lift and drag coefficients on the flat plate. The sinusoidal motion has an earlier stall than the linear-ramp motion. No

15. SUBJECT TERMS

Computational Fluid Dynamics, Flapping Wing

16. SECURITY CLASSIFICATION OF:			**17. LIMITATION OF ABSTRACT**	**18. NUMBER OF PAGES**	**19a. NAME OF RESPONSIBLE PERSON**
a. REPORT	**b. ABSTRACT**	**c. THIS PAGE**			**19b. TELEPHONE NUMBER** *(include area code)*

Standard Form 298 (Rev. 8-98)
Prescribed by ANSI Std. Z39.18

Numerical Investigation of a Low Aspect Ratio Flat Plate

Final Report

for

AFOSR Grant FA9550-09-01-0622

Research Area: Flow Interactions and Control

Submitted to Dr. Douglas R. Smith AFOSR/RSA

Tel: (703) 696-6219 Fax: (703) 696-7320

DSN 426-6219 Email: douglas.smith@afosr.af.mil

PI: Yongsheng Lian
University of Louisville
200 Sackett Hall, Louisville, KY 40292
Tel: (502) 852-0804
Email: y0lian05@louisville.edu

1. Abstract

This report presents the key findings resulting from an AFOSR grant. In this reseasrch we extended our previous results on the linear pitch-ramp-return of a two-dimensional (2D) flat plate to that of a three-dimensional (3D) flat plate of various aspect ratios, in an attempt to quantify 3D effects and the boundary effects on flapping wing aerodynamics. Specifically we compared the leading edge vortex (LEV) between the two-2D and the corresponding 3D cases, and the vortex structure and force histories between a small and a large computational domain. The computational approach solved the incompressible Navier-Stokes equations using a Poisson-like method on overlapping grids. In the computation, the impact of domain size and the presence of walls (as in the experiment) were investigated in particular detail, as earlier work on high-frequency pure-plunge cases has shown remarkable sensitivity of forces to domain size, as well as large differences between wall-bounded and unbounded flows. Comparisons were made with experiments performed at the Air Force Research Laboratory at Wright Patterson. Our study showed that a smaller domain leads to higher lift and drag coefficients on the flat plate. The sinusoidal motion has an earlier stall than the linear-ramp motion. Non-circulatory loads were found to be localized to phases of motion where acceleration is large. The low aspect ratio wing was seen to have slight difference in leading edge vortex evolution relative to that of the two-dimensional case.

2. Background and Rationale

Aiming to enhance the collaboration among different research groups and to identify the prominent features presented in the unsteady aerodynamics of flapping wing based micro air vehicles (MAVs), the AIAA Fluid Dynamics Technical Committee (FDTC) recently suggested a canonical case with simple geometry but rich phenomena pertinent to flapping wing MAVs. The idea is to repeat a test classical, but still establishing a common baseline across the various experiments and computations, matching the reduced frequency, pitch angle range and model geometry—but not Reynolds number. The group seeks to explore the question of putative Re-insensitivity in vortex shedding and aerodynamic load for small convective time after motion onset. The case is to study the aerodynamics of a flat-plate of 2% thickness with round leading and trailing edges and infinite-span. The plate starts at angle of attack (AoA) of zero degree and linearly pitches up to the maximum pitching angle. Two special sections had been devoted to this canonical case in the recent AIAA conference meetings.

Among others, Ol [2008] experimentally studied a wall-to-wall flat plate in the water tunnel. He systematically investigated the effects of pitch rate, location of the pitch pivot point, and the Reynolds number. He noticed that as the reduced pitch frequency increases, the LEV becomes more compact and is better able to retain its integrity as it eventually convects downstream. He also noticed that as pivot point further aft, the vertical extent of the wake becomes smaller. From his experiment, the Reynolds number effect is secondary at most. Garmann and Visbal [2009] numerically studied the canonical case using an implicit large-eddy simulation. Their parameter

study showed the airfoil geometry had a minimal effect on the integrated load. However, the small perturbations early in the motion caused significant changes in the development of the flow field around the airfoil. They suggested that the numerical simulation should use data from the measured displacement data due to vibration and lag in drive mechanisms to match the aerodynamic loads from the experiment. Hence it is critical to study different smoothing transients to understand the transient effects.

For the canonical case the upstroke is hypothesized to be fairly quasi-steady, i.e., lift follows angle of attack, except for the so-called "non-circulatory" loads associated with acceleration (of the model, and thus of the surrounding fluid). The hold and downstroke are expected to feature strong lags in aerodynamic response because of the residence of large leading edge vortices (LEVs) as they convect downstream over the plate's suction-side, and as various other vortices are shed to maintain the net circulation budget at zero. Questions to explore in parameter studies include putative Re-insensitivity in vortex shedding and aerodynamic loads, trends with reduced frequency, pitch pivot point location, pitch-plunge comparison, and acceleration transients. Preliminary results were summarized by Ol et al. (2010). As the reduced pitch frequency increases, the LEV becomes more compact and is better able to retain its integrity as it eventually convects downstream. As pivot point further aft, the vertical extent of the wake becomes smaller. Reynolds number, in the range of 1000-40,000, was found to have minimal effect on the flowfield evolution.

Another pertinent question is how the blockage/computational domain affects the flow field and forces. Most numerical simulations assume that the airfoil/wing is immersed in an unbounded fluid; however, during experiments, it is in a bounded fluid. When the flapping wing is close the walls, the walls surely have an impact on the wing aerodynamics such like the ground effect. The wall effect becomes more prominent when the wing is only a few chords away from the walls and the wing has a high frequency motion. For example, Anderson et al. [1998] used a towing tank that was 2.5 m wide and 1.2 m deep while the wing had a chord of 10 cm and span of 60 cm. Simulations from different groups using various CFD packages show large disagreements with experimental measurements (**Figure 1**). It seems that the simulations under predict thrust. Ol [2007] tested a flapping rectangular wing in a water channel. At the closest point, the wing came within less than 2-chord lengths away from the top and bottom surfaces. Koochesfahani [1989] performed an experiment for a 2D NACA0012 airfoil sinusoidally pitching about the quarter-chord point. The experiment was conducted in a low speed channel with a 50 cm-wide and 76 cm-deep test section. The test wing had a chord of 8 cm. The experiment was run with pitch amplitudes of 2^o and 4^o, and a reduced frequency ranging from 1.0 to 12. He calculated the mean thrust coefficient by measuring the momentum of the time-averaged velocity profiles on a control volume. His results showed noticeable differences compared to other simulated solutions, especially at high reduced frequencies. Ramamurti and Sandberg [2001] concluded that Koochesfahani's experiments increasingly over-predicted the thrust with increasing pitching frequency, citing the ignorance of the unsteady effects and

pressure differences on the control volume. Using a more complete control volume, Bohl et al. [2009] conclude the streamwise velocity fluctuations and pressure term were responsible for the over-prediction. Lian [2008] numerically studied a flapping airfoil. His results showed that forces were influenced by the size of the boundary. His simulations showed that as the reduced frequency increases, the boundary effect on the aerodynamic forces became more significant. He showed that a smaller computational domain leads to a much higher thrust coefficient on a plunging airfoil.

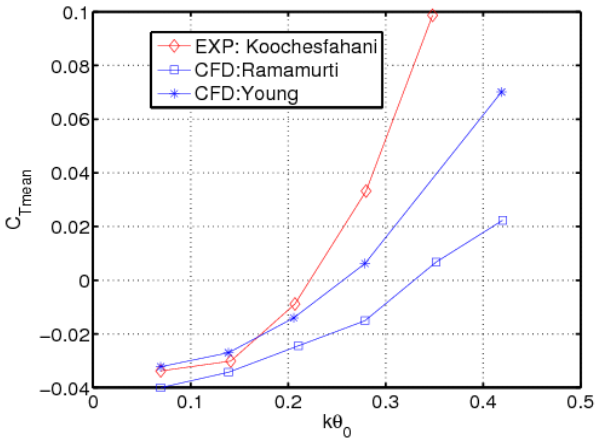

Figure 1. Comparison between experimental and numerical solutions for a pitching airfoil. The difference increases with the reduced frequency and pitch angle.

3. Computational Setup

3.1 Numerical Method

The flow field was simulated by solving the incompressible Navier-Stokes equations in curvilinear coordinates. For clarity, we present the governing equations in Cartesian coordinates

$$\square(\vec{u}_t + \vec{u}.\nabla\vec{u}) = -\frac{1}{\rho}\nabla p + \nu\nabla^2\vec{u} \tag{1}$$

$$\nabla.\vec{u} = 0 \tag{2}$$

Where $\vec{u}$ is the velocity vector, ρ is the density, p is the pressure, and ν is the kinematic viscosity. The equations were discretized on an overlapping grid using a second order accurate central difference approximation of the velocity and pressure equations. Time stepping was accomplished using a second-order accurate split-step scheme with an Adam's predictor corrector time-stepping method [Henshaw and Petersson, 2003]. For the Reynolds number considered, 5,000, the flow was assumed to be accurately modeled as a direct numerical simulation and no turbulence model was employed.

The overlapping moving grid was adopted to handle the dynamic motion of the wing [Henshaw 1994]. This method uses boundary-conforming structured grids to achieve high-quality representations of boundaries. It employs a Cartesian grids as the background grids so that the

efficiencies inherent with such grids can be exploited. The irregular boundary associated with standard Cartesian grid methods takes the form of the interpolation boundary between overlapping grids. The use of overlapping grids is desirable for moving bodies because it is computationally less expensive than most other conventional approaches. Interpolation points are located in the overlap region between different grids and are used to couple the solutions. As the body moves, the grid moves with it, meaning that only the interpolation points between grids must be recalculated as opposed to the need to regenerate the whole mesh, as may be necessary with other methods. A sample overlapping grid is shown in Figure 2. The background Cartesian grid and body-fitting curvilinear grid are represented by blue and green colors respectively. At the overlapping boundary, the interpolation points are marked with solid square symbols. The geometric conservation law [Thomas and Lombard, 1979] is enforced to update the Jacobin matrix.

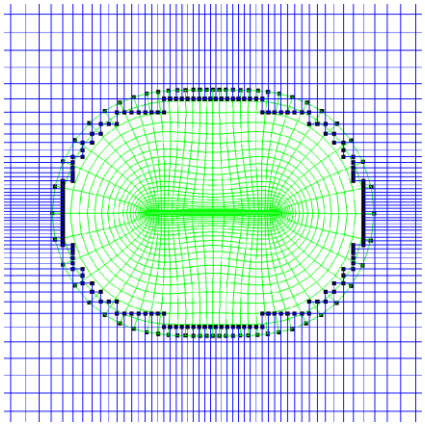

Figure 2. Sample overlapping grid. Blue color represents the background Cartesian grid and green color represents the body-fitting curvilinear grid. The solid square symbols represent the interpolation points.

3.2 Motion Defination

The baseline geometry is a flat plate of nominally 2.5% thickness and round leading and trailing edges. The round edges are intended for simplicity of model construction and computational gridding. The basic kinematics is an unsmoothed trapezoidal motion with pitch pivot point at the leading edge. The trapezoidal motion is smoothed to avoid vibration in experiments and instabilities in the computations. A C^{∞} smoothing function developed by Eldredge et al. (2009) is used:

$$G((t) = \ln \frac{\cosh(aU_{\infty}(t-t_1)/c)\cosh(aU_{\infty}(t-t_4)/c)}{\cosh(aU_{\infty}(t-t_2)/c)\cosh(aU_{\infty}(t-t_3))} \tag{3}$$

where a is an adjustable smoothing parameter, c is the chord length, and t_1 through t_4 are times defined as follows:

t_1 = time from start until when the sharp corner of the unsmoothed ramp would start
t_2= t_1+time duration of the ramp up, until the sharp corner when the hold would begin
t_3=t_2+the unsmoothed hold time at maximum angle of attack
t_4=t_3+the unsmoothed ramp down duration

The maximum pitch amplitude *A* is 45 degrees, and the smoothed motion becomes

$$\alpha(t) = A\frac{G(t)}{\max G(t)} \tag{4}$$

Varying the parameter *a* leads to different smoothing functions: a large one approximates the unsmoothed trapezoidal motion while a small one approximates a sinusoidal function. Figure 3 shows the time-trace of pitch angle obtained with two different *a* values. Setting *a*=11 produces a close fit to trapezoidal function and, *a*=2, the sinusoidal function.

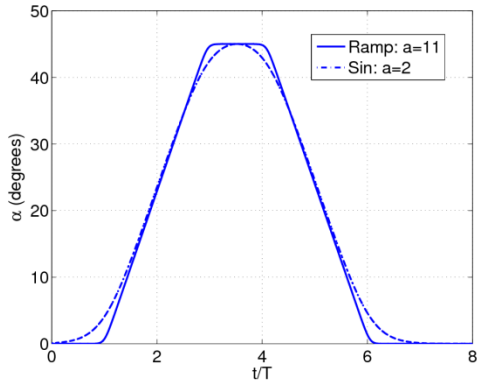

Figure 3. Time-trace of pitch angle. $T = c/U_\infty$ is the convective time.

In the trapezoidal motion, a dimensionless ramp rate, $K = c\dot{\theta}/2U_\infty$, is set to 0.2, where $\dot{\theta}$ is the linear pitch up rate. The hold time is about 1.12 times of the convection time (c/U_∞). The Reynolds number based on the wing chord and freestream velocity is 5,000. At this Reynolds number we assume flow is laminar.

4. Results

4.1 Grid Sensitivity Analysis

We begin with a grid sensitivity analysis. The computational set up attempts to match the experiment at least in 2D. In the water tunnel, the flat plate spans wall-to-wall and is 2-chords below the free-surface and 2-chords above the test section bottom, in its rest position. Three grid systems are compared. In the overlapping grid configuration, a curvilinear O-grid is generated around the flat plate and a rectilinear grid is used as the background grid. For the O-grid, the coarse grid consists of 150x90 grid points, the medium grid has 220x120 and the fine grid has 330x150. Both the ramp and sinusoid motions are tested but here we report the ramp motion

results only. Figure 4 shows the lift and drag coefficients. Refining the grid from coarse to medium shows clear improvement in both the lift and drag coefficients, but a further refinement to fine grid does not show much change during the upstroke and hold periods. The difference in the downstroke is still clear between the medium and fine grids. However, further grid refinement does not produce a converged solution. It seems that a convergence is difficult to obtain during the downstroke. Similar behavior is observed in other tests (Lian, 2009).

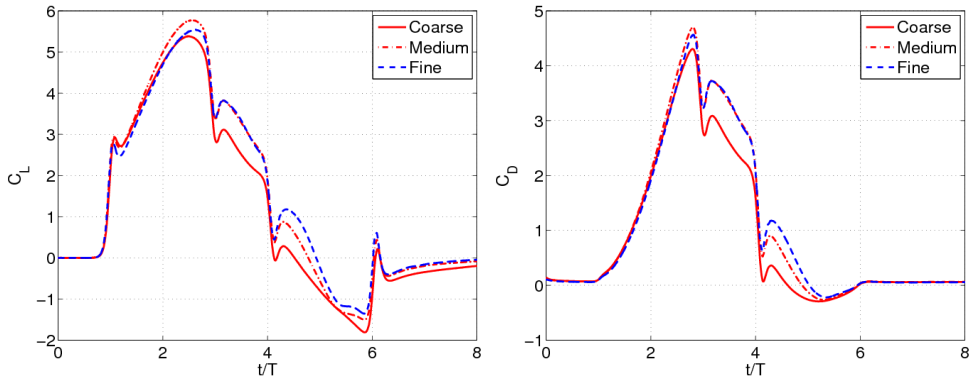

Figure 4. Lift and drag coefficients with different grids. Ramp motion with pivot point at the leading edge. The airfoil is initially about 2-chord away from the top and bottom walls. Re=5000.

The vorticity contours are compared in Figure 5, for the snapshot at the onset of the hold. Clear improvement is obtained when the grid is refined from coarse to medium. In addition, the medium grid is able to capture the leading edge vortex, the trailing edge vortex, and the shear layer vortex. For the 2D study, the medium grid is used throughout this paper.

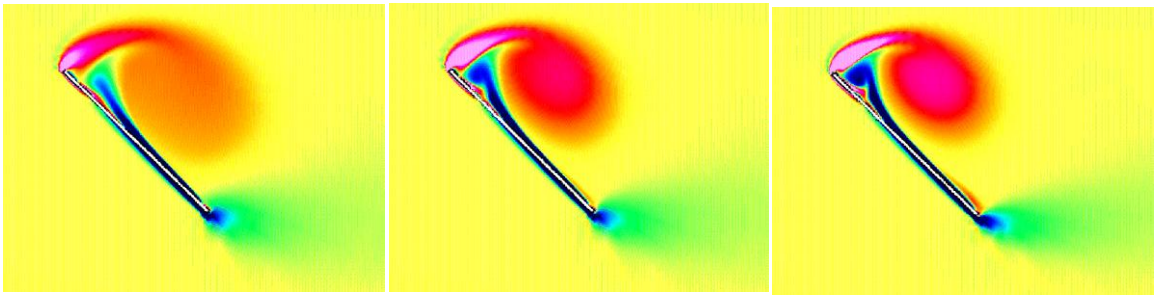

Figure 5. Comparison of vorticity contours on different grids. From left to right: coarse, medium, and fine. Snapshot at pitch-history midstroke ($\alpha = 45^o$).

4.2 Effect of Computational Domain Size, and Tunnel Upper/Lower Walls

As an open-jet water tunnel is somewhat impractical, wall effects raise questions of interference. Typically, one is concerned with effective span, in the sense of whether a nominally wall-to-wall model nevertheless has lower lift curve slope than the truly 2D case. Ol et al. (2009) found a static lift curve slope for a wall-to-wall model to be very close to $2\pi\alpha$. While it is possible that such apparently very close agreement with 2D theory is from fortuitous cancellation of errors,

such as tip losses vs. wake blockage[i], here we consider a possibly larger problem, of an upper and lower impermeable boundary above and below the model, but of infinite span. Thus the computational analog is 2D but with upper and lower boundaries to mimic the water tunnel's bottom and free-surface, but ignoring the sidewalls.

In most computations the far-field boundaries are usually more than 10 chords away from the model. But in the present experiments, the test section height is 4 chords (± 2 chords). To see how domain size affects this case, four different domains are tested. Figure 6 shows that the ± 2-chord domain size produces much higher coefficients than the other three; there is a roughly 50% overshoot relative to the lift predicted using the largest domain. The domain size effect almost diminishes when the outer boundary is more than 10 chords away from the flat plate. The observation of 50% overshoot in lift between the largest domain and the domain intended to represent the water tunnel, is borne out by the close agreement between the lift computed on the domain intended to match the water tunnel test section height, and the experimentally measured lift (Figure 6, right-hand portion, dark gray curve). Experimental-computational agreement is best on the upstroke and somewhat worse on the downstroke, evidently because of (1) insufficient grid resolution to capture fine separated structures, and (2) the 3D spanwise nature of these structures, to which a 2D computation is incapable of capturing; the same observations were reported by Ol et al. (2010) for two different computations. We also note that the computation under-predicts the non-circulatory spikes in lift coefficient, relative to experiment – and this is independent of domain size. Evidently the cause is again insufficient density of the grid.

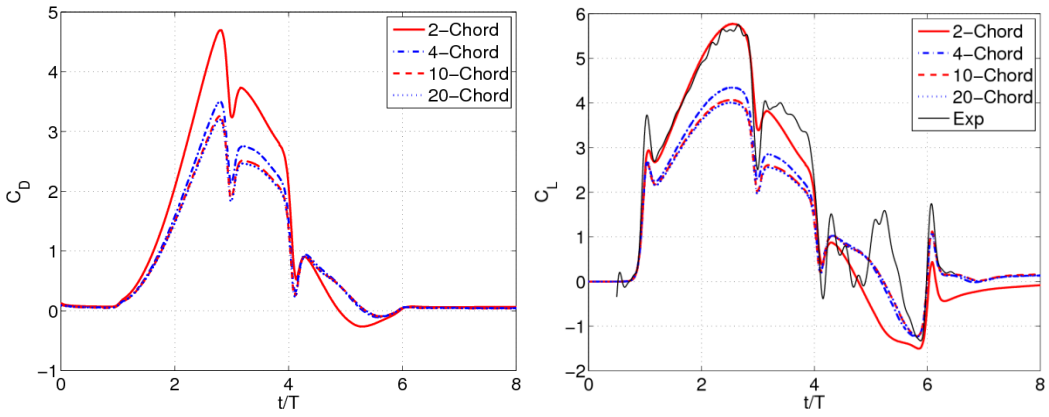

Figure 6. Effect of computational domain size on aerodynamic coefficients (drag, at left, and lift, at right); ramp motion at Re=5000.

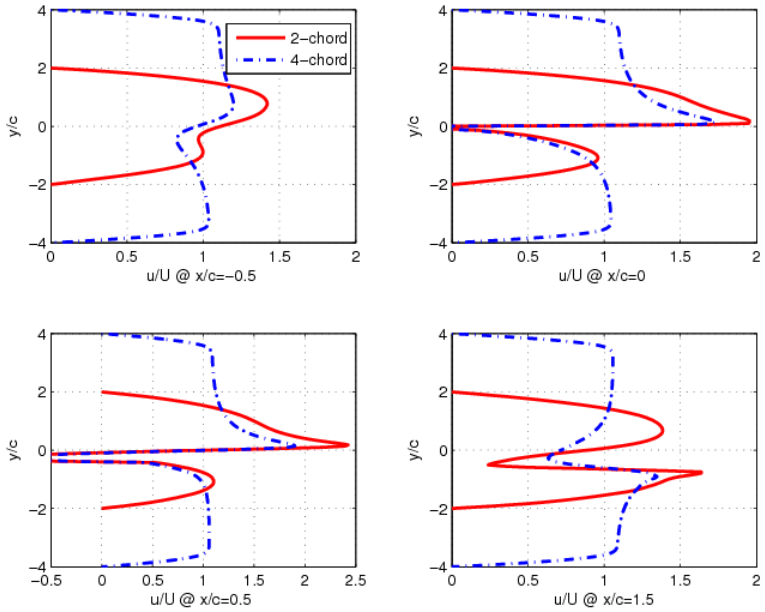

Figure 7. Wake velocity profiles for different computational domain sizes; ramp motion, Re=5000.

The role of computational domain size can be further elucidated by considering wake velocity profiles. Figure 7 compares computed wake velocity profiles at four different cross sections. In each cross section, the smaller domain produces higher jet-like spikes of velocity due to larger blockage and its local accelerating effect on the flow. In the following, we limit the computational results to the ± 2-chord domain.

4.3 Ramp Motion vs. Sinusoidal Motion

Compared to the ramp motion, the sinusoidal motion is smoother, which is reflected in the lift coefficient history shown in Figure 8. In the ramp motion the lift coefficient abruptly increases to 2.5. After a local spike associable with non-circulatory lift, it them ramps up to 5.5 with a lower slope. "Stall" occurs at about 37 degrees, before the plate reaches its maximum angle of attack of 45 degrees. After stall, lift shows a sudden drop, followed by another spike associated with the onset of the hold, and then decreases with a lower slope. On the downstroke the lift decreases below zero even while the angle of attack is positive. The sinusoidal motion produces a lift time history devoid of non-circulatory spikes, but the apparent lead between lift and alpha history is again due to the acceleration at motion onset. Stall occurs at a lower angle of attack, of around 30 degrees; and maximum lift coefficient is marginally lower.

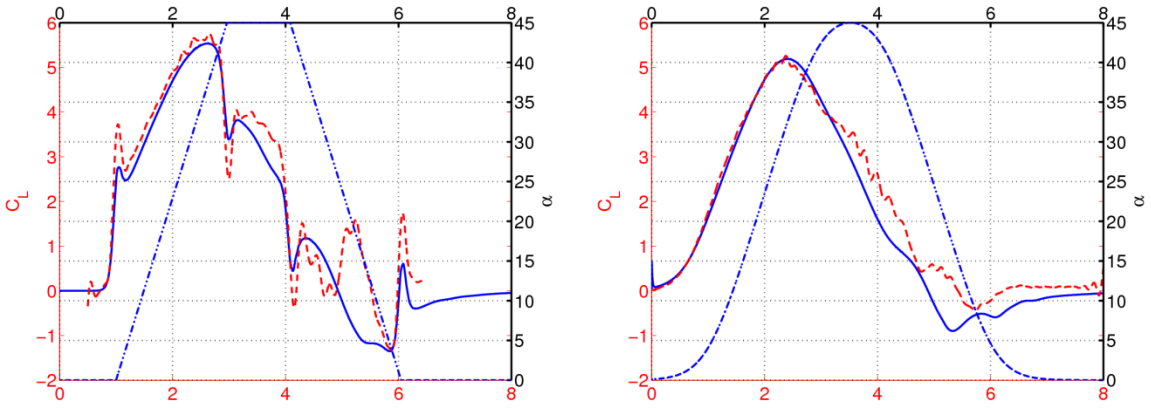

Figure 8. Comparison of lift coefficient between the ramp motion and sinusoidal motion: experiment (dashed red curve, and computation (solid blue curve).

In Figure 9 we compare the vorticity contours for the ramp and sinusoid late in the upstroke, at the motion midpoint, and early in the downstroke. In the downstroke the two motions evince very similar flowfields, with the LEV having pinched off and convecting downstream, and a trailing edge vortex (TEV) of opposite sign forming in both cases. But the LEV for the two motions is somewhat different; for the sinusoid, it is spatially larger and more diffuse, evidently because the smoother pitch acceleration and therefore a weaker pressure gradient at the leading edge, which would ultimately be responsible for the LEV. The analogous dye injection in Figure 10 shows very little difference between ramp and sinusoid LEVs, but there is a flowfield difference at the moment of motion cessation: the ramp, with a more abrupt stop, evidently sheds a stronger stopping vortex.

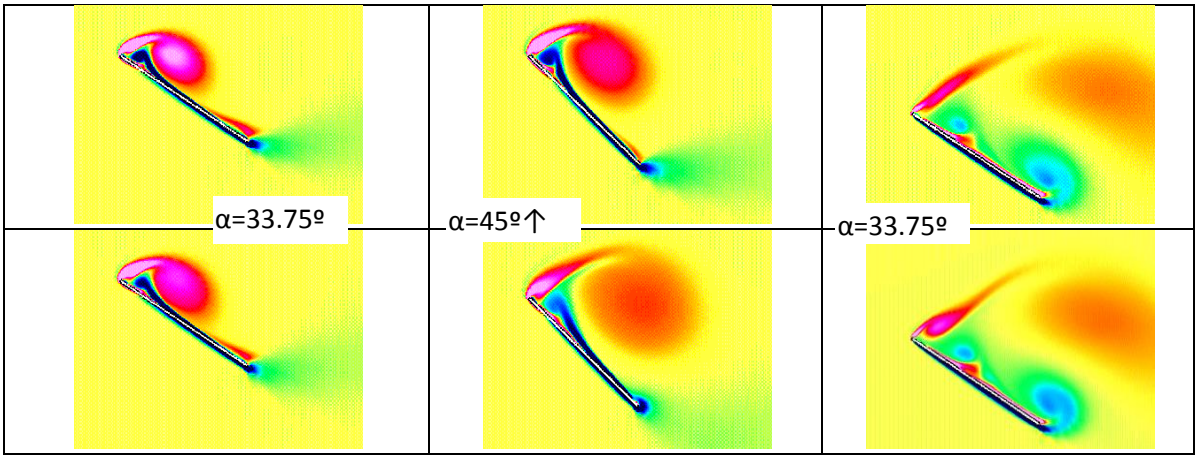

Figure 9. Comparison of vortex contours between ramp (top row) and sinusoid (bottom row) motions. From left to right: α=33.75º on the upstroke; the motion midpoint (α=45º); and α=33.75º on the downstroke.

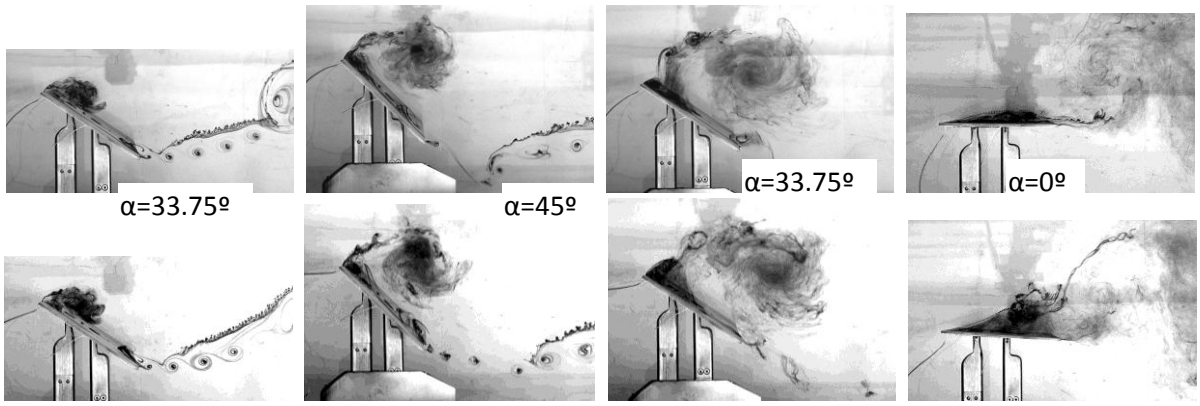

Figure 10. Comparison of dye injection between ramp (top row) and sinusoid (bottom row) motions. From left to right: α=33.75º on the upstroke; the motion midpoint (α=45º); α=33.75º on the downstroke; and at motion cessation (α=0º).

4.4 Effect of Pitch Pivot Point Location

We next consider different pitch pivot points. The lift and drag coefficients are shown in Figure 11 and the flow structures are compared in Figure 12. When the pivot point is at the trailing edge, two positive spikes appear in both the lift and drag histories, at the endpoints of the high-alpha hold. The difference between the leading edge pivot and quarter chord pivot is relatively small. Moving the pivot point toward the trailing edge also delays the formation of the LEV. Further, the trailing edge vortex becomes less prominent. Overall, the CFD vorticity contour plots show fairly good agreement with the dye injection results.

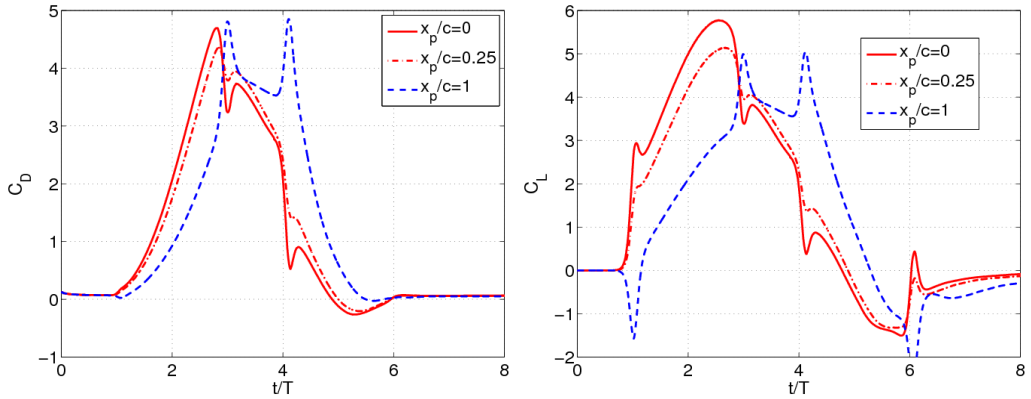

Figure 11. Comparison of aerodynamic coefficients for different pivot points (x/c = 0, 0.25 and 1.0) for the ramp motion.

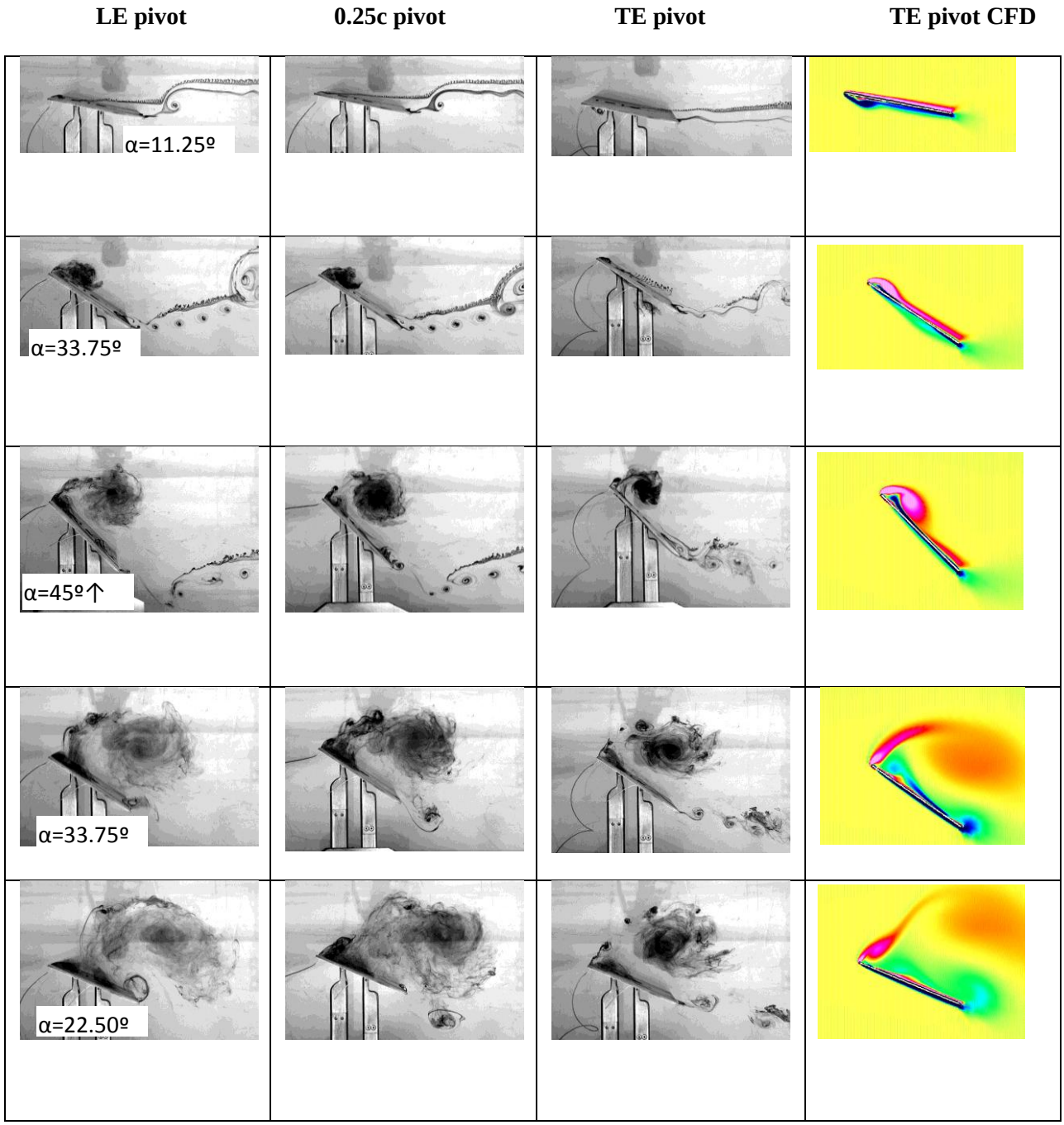

Figure 12. Comparison of wall-to-wall plate ramp-motion flowfields, experiment and computation; dye injection, pivot about the leading edge (left column), quarter-chord (2nd column), and trailing edge (3rd column). Computation, pivot about the trailing edge (rightmost column).

4.5 AR=2 vs. Wall-to-Wall

We now turn to the 3D simulation, for an aspect ratio 2 flat plate, with round edges. The reported results use a grid size of 125x36x25. It is expected that this grid is not sufficient to capture the detailed flow structure. However, it still can reveal qualitative difference between

the wall-to-wall case (computed in 2D) and the AR=2 case. Figure 13 compares the vorticity contours between 2D and 3D at two different sample planes. Similarly, Figure 14 shows dye injection snapshots for the wall-to-wall plate and the AR=2 plate at three sample planes: midplane, halfway towards the starboard side (3/4-span) and three-fourths towards the starboard side (7/8-span). In the experiment, the AR=2 plate's chord is 117mm, whereas the wall-to-wall plate's chord is 152.4mm. But in Figure 14, images have been scaled to render the two models' chords of same size. Iso-surfaces of computed vorticity in 3D rendering are shown in Figure 15. And planform views of dye injection, from a port at the 3/4-span location along the leading edge, are given in Figure 16.

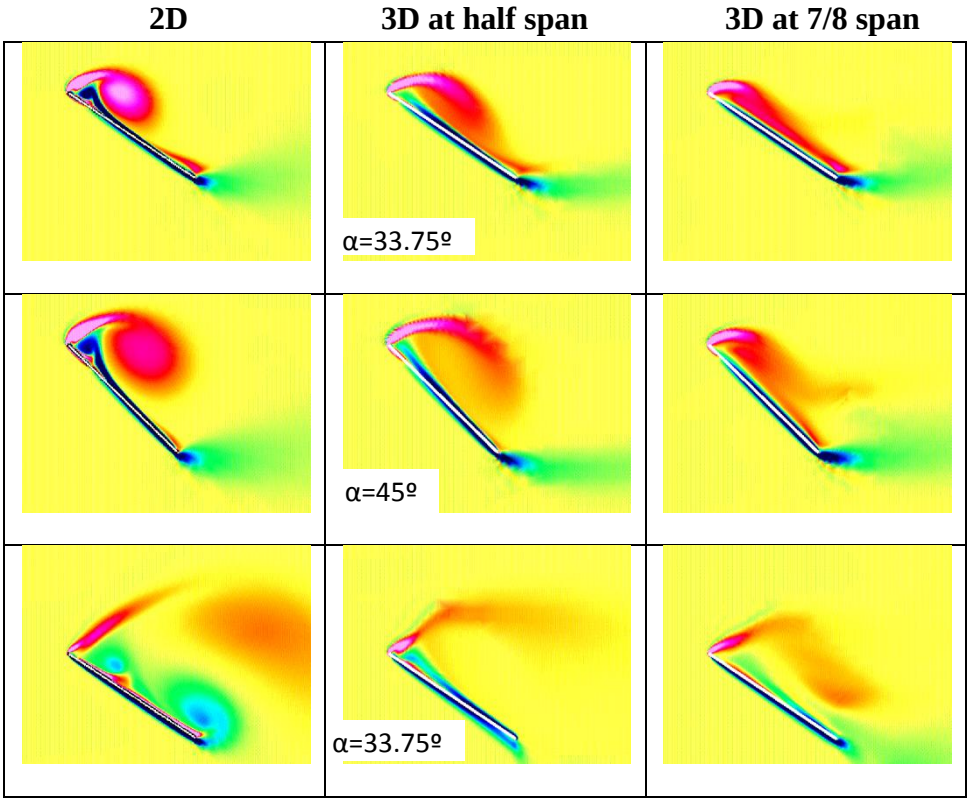

Figure 13. Comparison of vorticity contours between 2D and 3D computational results, at the late upstroke (top row), motion midpoint (middle row) and early downstroke (bottom row).

Computation finds more difference between the wall-to-wall plate and the AR=2 plate, than does the experiment. Dye injection at α=22.5º on the upstroke, for example, shows a similar LEV for the wall-to-wall plate and for the AR=2 plate, at every spanwise sampling location. At α=33.75º on the upstroke and later in the hold portion of the motion, the dye streak associable with the LEV for the wall-to-wall plate does indeed begin to look larger than for the AR=2 plate, and differences accentuate during the downstroke. Results from midplane injection for the AR=2 plate retain more similarity to the wall-to-wall case, while going further outboard, one finds marginally less standoff for the vestiges of the LEV of the AR=2 plate on the downstroke. The

computation, on the other hand, shows a strong coherent LEV for the wall-to-wall plate at the motion midpoint, but a structure more akin to a shear layer for the AR=2 plate.

Both experiment and computation find no reason to assert that the AR=2 plate produces a more stable LEV than does the wall-to-wall plate. If anything, the observation is to the contrary.

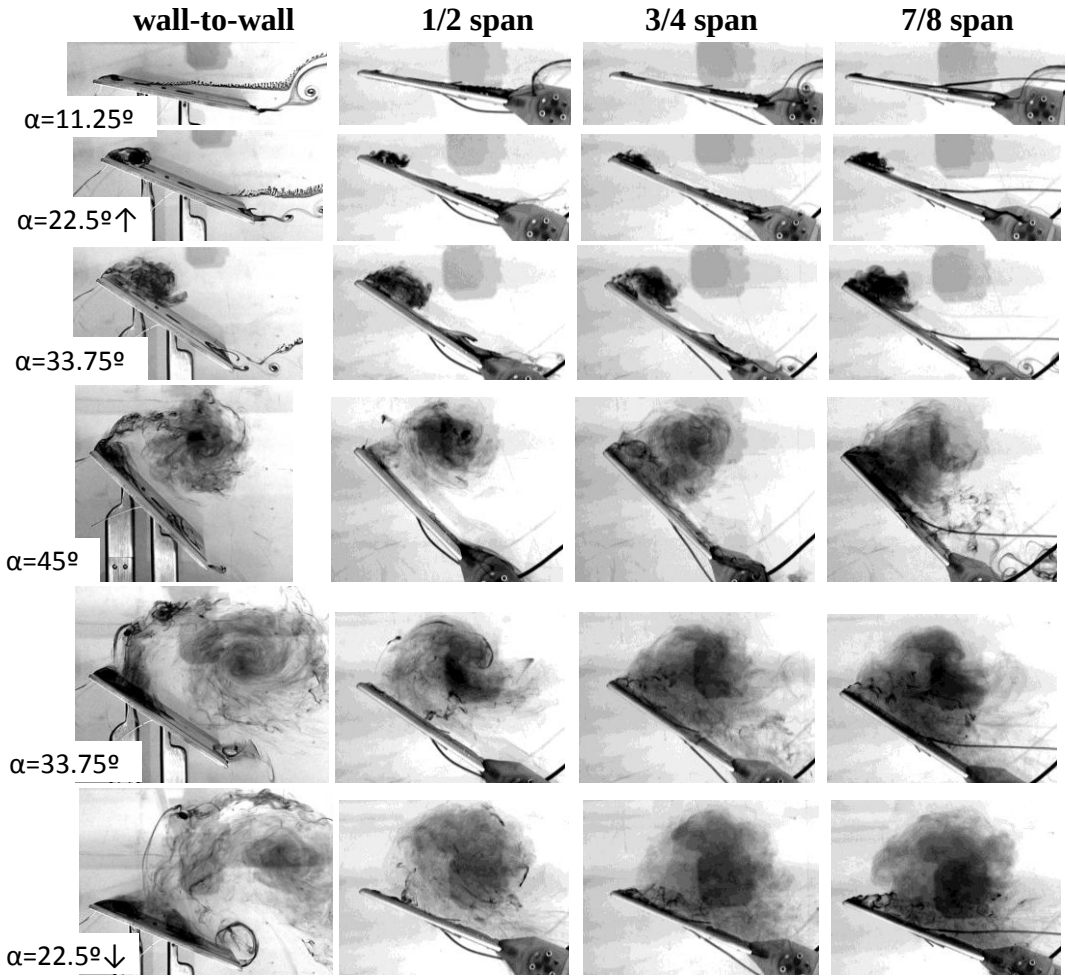

Figure 14. Dye injection for ramp motion of wall to wall plate (left column) and AR=2 plate: injection point at midspan (2nd column), 3/4 span (3rd column) and 7/8 span (4th column).

In the side views presented so far, we have been liberally confident that dye streaklines are a reasonable proxy for vorticity, and that 2D or sectional views of computed vorticity contours can readily be associated with side views of the wing dye injection. Isometric view of vorticity iso-surfaces however do not compare as readily with planform views of dye injection, as the latter really are a single-point-source method, while the former are limited to one contour level. So comparison of vorticity and dye concentration depends on deft (or lucky) choice of contour levels. This is beside the usual observation that vorticity is a vector, while dye concentration is a scalar – and moreover a scalar of nonnegative value. That said, one can observe that early on the upstroke in Figure 15, the LEV formation is largely two-dimensional, except for the close vicinity of the tip vortices. As angle of attack increases, the LEV becomes increasingly varying

along the span. Early in the downstroke the vortical structure associable with the chosen iso-surface has appeared to pinch off, and even by the completion of the motion, a large flow separation remains. In the dye injection, we observe a thin organized streak early in the upstroke, indicative of little or no spanwise flow. But by halfway up the upstroke, an LEV-type structure develops with growing spanwise extent. The dye initially moves inboard, towards the model's centerplane. During the downstroke, the spanwise direction of the dye streak shifts towards outboard, and by the completion of the motion, the dye streak is clearly entrained into the path of the tip vortex. As in the computation, the flow remains separated.

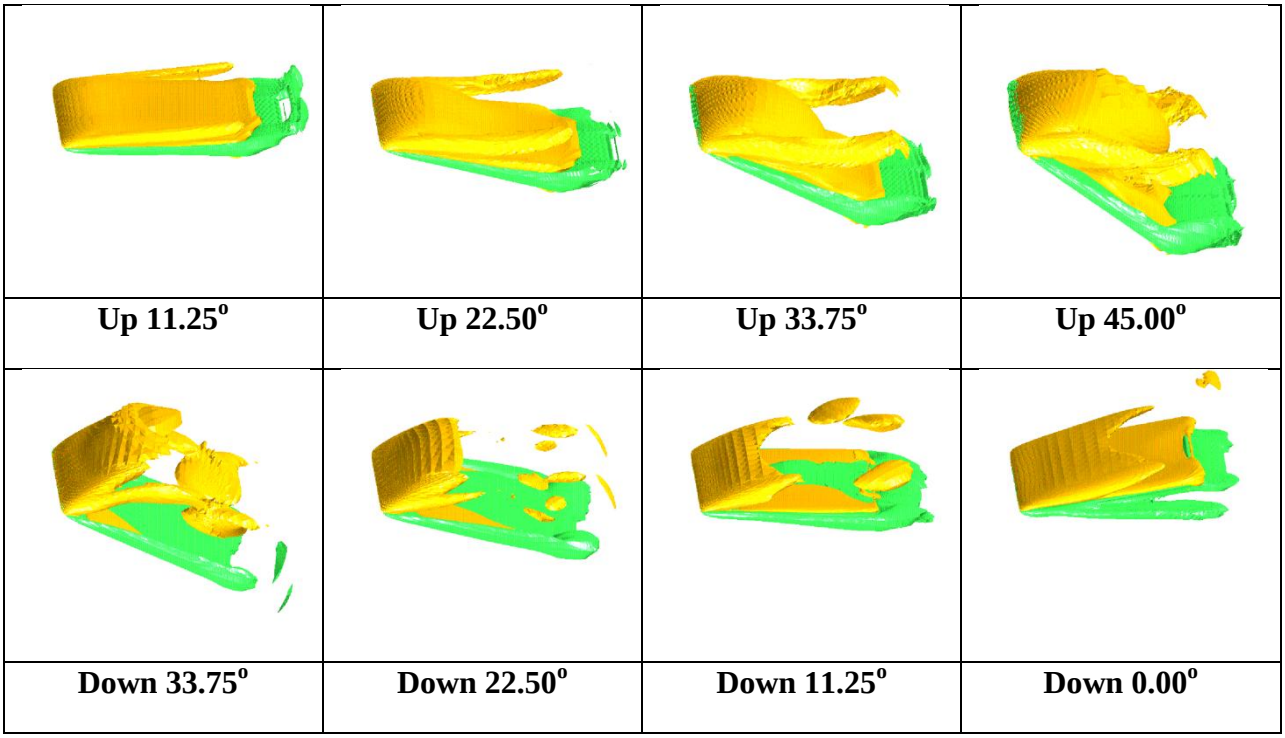

Figure 15. Iso-surface of computed vorticity contours.

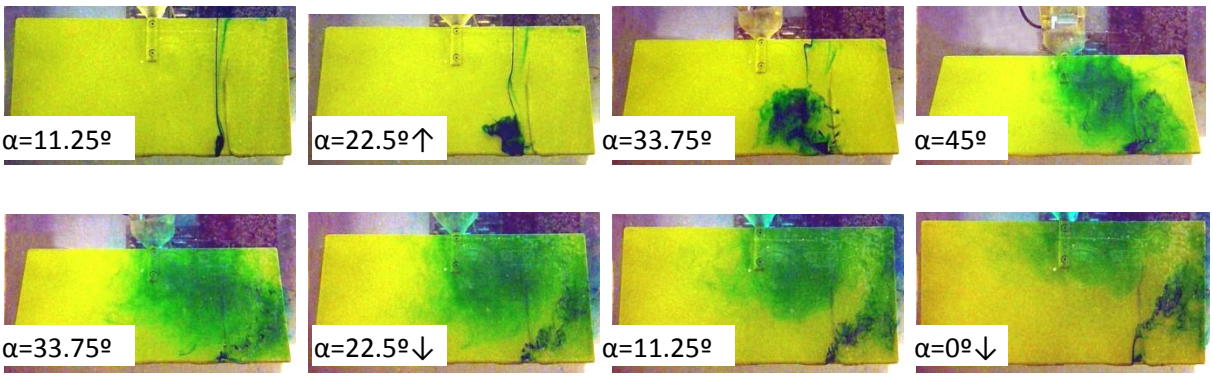

Figure 16. Dye injection at 3/4 span of leading edge, AR=2 plate, ramp motion, Re = 5000. Instantaneous angle of attack as marked, leading edge towards bottom of each image, and flow direction from bottom to top of each image.

Despite the clear presence of tip vorticies for the AR=2 plate, we do not find definitive evidence that the inboard flowfields between the AR=2 and wall-to-wall plates differ greatly. Of course, a more thorough analysis would require quantitative 3D visualization of the experimental conditions, and higher resolution in the computation.

5. Conclusion

Computed vorticity contours and snapshots of leading-edge dye injection in a water tunnel experiment give reasonable qualitative agreement of flowfield features for high-alpha high-rate transient motions of flat plates. A computational study of domain size, intended to model the upper and lower bounds of the water tunnel test section, found a blockage-like effect where apparent lift coefficient is some 50% higher in the bounded case than for that of a larger domain. This is consistent with experimental measurement of lift in the water tunnel using a fiber-Bragg balance is in excellent agreement with computation on a ± 2-chord domain. The effect of computational domain size, and presumably tunnel test section size, raises important questions of dynamic blockage – or at the very least, test technique – in wall-bounded highly unsteady experiments. Computational-experimental agreement was less successful for an AR=2 plate, with the former predicting large differences in leading edge vortex formation between low aspect ratio and 2D cases, but dye injection finding little difference. As is being reported in ongoing similar work, the role of non-circulatory spikes in lift, due to motion acceleration effects, is clearly evinced, and is intuitively consistent in comparison between a sinusoidal pitch ramp motion, which is always accelerating, and a smoothed ramp-type motion, where accelerations are large and confined to small periods of time. Further work is imperative on parameter studies of dynamic blockage, and high resolution 3D methods (computational and experimental) for low aspect ratio configurations.

Reference

Anderson, J.M., Streitlien, K., Barrett, D.S. & Triantafyllou, M.S., "Oscillating foils of high propulsive efficiency," *J. Fluid Mech.*, 360, pp. 41-72, 1998.

Bohl, D.G., and Koochesfahani, M.M., "MTV Measurements of the Vortical Field in the Wake of an Airfoil Oscillating at High Reduced Frequency," *J. Fluid Mech*. Vol. 620, pp. 63-88, 2009.

Eldredge, J.D., Wang, C.J., and Ol, M. "A Computational Study of a Canonical Pitch-up, Pitch-down Wing Maneuver". AIAA 2009-3687.

Garmann, D.J., and Visbal, M.R., "High-Fidelity Simulations of Transitional Flow Over Pitching Airfoils," AIAA Paper 2009-3693.

Henshaw, W.D., and Petersson, N. A., "A Split-Step Scheme for the Incompressible Navier-Stokes Equations," *Numerical Simulation of Incompressible Flows*, World Scientific, pp. 108-125, 2003.

Henshaw, D.W., "A Fourth-Order Accurate Method for the Incompressible Navier-Stokes Equations on Overlapping Grids,".*Journal of Computational Physics*, Vol. 113, pp. 13-25, 1994.

Henshaw, D.W., and Schwendeman, D.W., "Moving Overlapping Grids with Adaptive Mesh Refinement for High-Speed Reactive and Non-reactive Flow," *Journal of Computational Physics*, Vol. 216**,** pp. 744-779, 2006

Lian, Y., "Numerical Investigation of Boundary Effects on Flapping Wing Study," AIAA Paper 2009-539

Lian, Y., "Parametric Study of a Pitching Flat Plate At Low Reynolds Numbers," Invited AIAA Paper 2009-3688.

Ol, M., "Vortical Structures in High Frequency Pitch and Plunge at Low Reynolds Number". AIAA 2007-4233, 2007.

Ol, M. "The High-Frequency, High-Amplitude Pitch Problem: Airfoils, Plates and Wings," AIAA Paper 2009-3686, 2009.

OL, M.V., Altman, A., Eldredge, J.D., Garmann, D., and Lian, Y. "Résumé of the AIAA FDTC Low Reynolds Number Discussion Group's Canonical Cases". AIAA 2010-1085.

Pope, A. *Wind Tunnel Testing*. Chapter 6: "Wind-Tunnel-Boundary Corrections." Wiley, 1961.

Ramamurti, R. and Sandberg, W. C. "Simulation of flow about flapping airfoils using a finite element incompressible flow solver. *AIAA J.* **39**,253 -260, 2001.

Thomas, P. D., and Lombard, C. K., "Geometric Conservation Law and its Application to Flow Computations on Moving Grids," *AIAA Journal*, Vol. 17, No. 10, pp. 1030-1037, 1979.